A Novel Approach to Design Lesion-Specific Stents for Minimum Recoil

Muhammad Farhan Khan
PhD Student
Department of Mechanical, Materials and Manufacturing Engineering
Faculty of Engineering
University of Nottingham
University Park
Nottingham, UK
NG72RD
eaxmfk@nottingham.ac.uk
ASME Student member

David Brackett[2]
Research Fellow
Department of Mechanical, Materials and Manufacturing Engineering
Faculty of Engineering
University of Nottingham
University Park
Nottingham, UK
NG72RD
David.Brackett@the-mtc.org

Ian Ashcroft
Professor of Mechanics of Solids
Department of Mechanical, Materials and Manufacturing Engineering
Faculty of Engineering
University of Nottingham
University Park
Nottingham, UK
NG72RD
Ian.Ashcroft@nottingham.ac.uk

Christopher Tuck
Professor of Materials Engineering
Department of Mechanical, Materials and Manufacturing
Faculty of Engineering
University of Nottingham
University Park
Nottingham, UK
NG72RD
Christopher.Tuck@nottingham.ac.uk

Ricky Wildman[1]
Professor in Multiphase Flow and Mechanics
Department of Chemical and Environmental Engineering
Faculty of Engineering
University of Nottingham
University Park
Nottingham, UK
NG72RD
ricky.wildman@nottingham.ac.uk

ABSTRACT

Stent geometries are obtained by topology optimisation for minimised compliance under different stenosis levels and plaque material types. Three levels of stenosis by cross-sectional area, i.e. 30%, 40% and 50% and three different plaque material properties i.e. calcified, cellular and hypocellular, were studied. The raw optimisation results were converted to clear design concepts and their performance was evaluated by implanting them in their respective stenosed artery types using finite element analysis. The results were compared with a generic stent in similar arteries, which showed that the new designs showed less recoil. This work provides a concept that stents could be tailored to specific lesions in order to minimise recoil and maintain a patent lumen in stenotic arteries.

1 INTRODUCTION

Cardiovascular disease (CVD) is the main cause of death in England and Wales, with approximately 124,000 deaths per year, among which nearly half are due to atherosclerosis [1]. In atherosclerosis plaque is accumulated in the coronary arteries,

[1] Corresponding author.
[2] Current affiliation: The Manufacturing Technology Centre
Pilot Way, Ansty Business Park
Coventry, CV7 9JU
United Kingdom.

restricting the flow of oxygen-rich blood to the heart muscle. Treatment of these narrowed arteries mainly involves the placement of balloon-expandable stents, which are usually metallic wire mesh inserts that support and expand the diseased vessel, allowing blood flow to be restored.

Since their first use in 1986 [2], stents have evolved in terms of design, materials and drug coatings to achieve better post-implantation results. Presently, the main concern about this treatment is restenosis, or the re-blocking of the stented artery, normally known as in-stent restenosis (ISR). There are a variety of stent designs available, each differing with regard to material, strut thickness, coating and drug elution. It is known that stent varieties trigger different vascular responses and a number of desired attributes have been identified in the literature, including biocompatible surface material, thinner struts, modular design, low recoil and low material surface area [3–7]. Stenting is not risk free and poor stent design can contribute to re-blocking conditions, such as thrombosis and neointimal hyperplasia [8]. These adverse conditions mainly depend upon how the stent geometry interacts with the arterial surface and the resulting effects on blood flow.

Currently, stenting (stent deployment) of diseased arteries involves the use of “off-the-shelf” devices. This lack of personalisation raises the potential risk of suboptimal stent deployment in the target’s diseased vessel. This is particularly the case when treating diseased arteries with severely calcified plaques, which can result in low lumen area and shape.

It is known that with the progression of atherosclerosis, plaque composition and mechanical properties vary considerably and plaque histological types such as cellular,

hypocellular and calcified have been found to have statistically different radial compressive stiffness [9]. To take lesion properties, such as shape and stiffness, into account during stent design is, hence, of great importance. It was shown in a recent study of self-expanding stents [10] that lesion calcification of the arterial wall could lead to a more severe residual stenosis, dog-boning effect and corresponding edge stress concentrations after stenting. This ultimately could mean that the stent may not be able to serve its purpose-to adequately support the diseased artery. Zhao et al. [10] investigated soft and hard plaques, both causing a stenosis of 50%. After stent deployment, whilst the artery with the soft plaque experienced a residual stenosis of 15%, 39% residual stenosis still existed in the case with the stiffer plaque, which does not satisfy the allowable residual stenosis standard of 30% or less [11,12]. It is therefore vital to consider design changes to the stent to achieve acceptable lumen diameter in such calcified arteries.

In another study, Garcia et al. [13] investigated the design of a variable radial stiffness, self-expanding stent for a carotid artery with a calcified plaque. It was emphasised in their study that all desirable features in a stent are hard to achieve at the same time, therefore it is necessary to reach a compromise between tissue stress, stent flexibility and radial force. In their investigation they mainly focused on altering the strut thickness of the stent to achieve minimal contact pressure in the healthy region of the artery during expansion. Pericevic et al. [14] investigated the influence of plaque materials on a selected stent based on balloon-expandable design and concluded that plaque type has a significant effect on the stresses induced within an artery which may alter arterial response. These

studies provide the evidence of the impact of lesion types on the outcome of stenting procedure and demonstrate the need to develop customised stent geometries for specific lesion types.

In order to create customised stents, it is crucial to accurately measure and map the forces acting on stents exerted by complex lesions. Current procedure for arterial assessment involve intravascular ultrasound (IVUS) that mainly relies on acoustic reflections to determine plaque composition [15], other methods include computed tomography (CT) scanning [16], cardiac magnetic resonance (CMR) [17,18] and optical coherence tomography (OCT) [19]. However, advancements in arterial imaging and sensing technologies, and the conversion from images to *in silico* models will be necessary in order to benefit from customisation. Researchers have recently developed stretchable polymer-electronic balloon catheters from novel materials containing dense arrays of sensors and therapeutic modules [20,21]. These catheters could be used to provide information with high sensitivity about the local arterial microenvironment such as temperature, material type and force exerted by lesions. In this paper, we have used a similar concept by exploiting finite element analysis (FEA) and implanting a cylinder *in silico* into a set of stenotic arteries to extract the exact forces applied by the arteries to tailor stent designs using topology optimisation.

Recent studies [22,23] have suggested bioresorbable stents, commonly referred to as scaffolds, as a possible future option for coronary intervention. As a consequence, polylactic acid (PLA) was chosen as the material during the design process. Bioresorbable stents have the advantage of natural absorption by the body after functioning for the

required period of time. No longer being present in the body as a permanent implant, the risk of restenosis is reduced as well as allowing the artery to resume its beneficial natural vasomotion.

Topology optimisation (TO) is a type of structural optimisation method where the aim is to find the optimal material distribution and connectivity of structural elements [24]. Various approaches have been proposed for TO [25–33], which is gaining attention in a wide variety of applications. TO based contact analysis of stent and diseased artery is a novel approach to take into account the accurate loading conditions of different plaque types to customise stent architectures according to specific lesions while maintaining vessel lumen area. Although many groups have researched the biomechanical performance of stents using finite element methods [13,34–38], including very limited stent TO studies [39–41], topological optimisation has not been explored in the plaque-specific stent design fields. This paper aims to demonstrate that TO can be used to generate designs that enable recoil to be minimised even in conditions where there are strong variations in material property and surface topology of the lumen side of an artery, particularly in the axial direction.

2 METHODS

In this paper, a set of topologically optimised PLA stents were developed and their performance investigated and compared to a generic stent in terms of their radial deformation after implantation in a set of virtual stenosed arteries. The optimised stents are obtained through the solid isotropic material with penalisation (SIMP) [42] method of

topology optimisation. The proposed design method has three essential steps, as shown in Figure 1 and described below, and was carried out for each combination of plaque type and stent.

(i) A contact finite element analysis involving a stenotic artery of particular type and a cylindrical tube, representing the design domain for a stent topology. The extracted force from this analysis acts as a loading boundary condition for step (ii).

(ii) Topology optimisation of a stent, based on extracted contact normal forces from step (i).

(iii) Contact analysis of generic and optimised stents with the corresponding diseased artery for performance evaluation in terms of radial deformation.

A complete topology optimisation driven design process is illustrated in Figure 2, outlining the development and production of lesion-specific stents.

2.1 Geometric Models and Material Properties

The finite element models used in this study were developed using MSC.Patran and MSC.Marc was employed as the non-linear solver (MSC Software, Santa Ana, CA). Each stenosed artery was defined by two different parameters: stenosis level and plaque material type. With 3 stenosis levels: 30%, 40%, 50% by area and 3 plaque material types: calcified, cellular and hypocellular, hence, 9 different diseased artery models were created. The plaques modelled were eccentric and covered a length of 10 mm with maximum wall thickness of 0.66 mm, 1.0 mm and 1.24 mm corresponding to a stenosis of 30%, 40% and 50% respectively. Percent stenosis cross-sectional areas were calculated as: 100 x [1 – (Stenotic lumen area/Original lumen area)]. The artery was modelled as a

straight vessel with a length of 20 mm and inner radius of 2.22 mm. The thickness of atherosclerotic human coronary arteries range from 0.5 to 1.2 mm, depending on location [43]; in our study a thickness of 0.5 mm was chosen. Figure 3 illustrates XZ cut view of the stenotic arteries used.

Each simulation model was composed of two bodies, a diseased artery and a cylinder acting as a force sensing balloon catheter (or the generic stent for comparison with optimised designs). The generic stent (Figure 4) selected was inspired by the bioabsorbable Igaki-Tamai stent [44], and was chosen on the basis that it captured the main features of most commercially available designs, without being specific to a particular type. The cylinder used in each scenario, had outer radius of 2.57 mm (greater than the artery), length of 15mm and thickness of 0.2 mm. The generic stent had an outer radius of 2.45 mm and was assumed to be in a nearly expanded state. The material used for the generic stent and the force extracting cylinder was modelled as an elasto-plastic polylactic acid (PLA) polymer blend, having elastic modulus, E = 3.5 GPa, yield stress σ_y = 60 MPa and Poisson's ratio, v = 0.36, based on data in the literature [45–47]. The artery and 3 plaque types were modelled with a third-order non-linear hyperelastic material model, as suitable for an incompressible isotropic material. This has previously been found to adequately describe the non-linear stress-strain relationship of elastic arterial tissue, and is given by [48]

$$W = C_{10}(I_1-3) + C_{01}(I_2-3) + C_{20}(I_1-3)^2 + C_{11}(I_1-3)(I_2-3) + C_{30}(I_1-3)^3 \quad (1)$$

where W is the strain-energy density function of the hyperelastic material, I_1, I_2 and I_3 are the strain invariants and C_{10}, C_{01}, C_{20}, C_{11}, C_{30} are the hyperelastic constants. Table 1

summarises the constants used for the hyperelastic constitutive equations to define the 4 material types.

2.2 Meshing and Boundary Conditions

Eight noded first order hexahedral, full integration elements were used to mesh all the atherosclerotic artery models. Mesh convergence studies, as shown in Figure 5, were carried out for one of the artery models to select an appropriate mesh size. The results demonstrate that 41760 elements in the artery and plaque are a reasonable compromise between accuracy and computational efficiency. The cylinder used for contact normal force sensing was modelled as a shell mesh of 6804 quad 4 elements. This was also used as the design domain for stent optimisation. The generic stent consisted of 6849 quad 4 shell elements.

The boundary conditions applied were comprised of an internal pressure, displacement boundary conditions and contact. The artery and cylinder/stent were constrained axially and allowed to expand and contract radially. The cylinder/stent in each case was first positioned inside the artery with elements, as shown in Figure 6, deactivated. The vessel was then inflated by applying pressures of 32.5 MPa for 30% and 40% stenosis and 65.05 MPa for 50% stenosis. These pressure values expanded the corresponding arteries enough such that the slightly oversized cylinder could be positioned inside or “implanted.” This process was carried out in two load case steps; first, the cylinder elements were deactivated from the contact table such that the artery could expand freely. In the second step, cylinder elements were activated in the contact table, pressure was then reduced to diastole (0.013 MPa) such that the artery wrapped around the

cylinder. For the analysis involving generic stent, internal pressure was applied to stent initially to expand and plastically deform while stenotic artery elements were deactivated. The pressure was then removed to allow the stent to recoil and achieve its final diameter of 5.15 mm. The stenotic artery in each case was then inflated and deflated in the last load case to wrap around the stent as performed in previous analyses. Contact between artery models and the cylinder was defined as deformable-deformable 'touch' contact. All the artery models were solved for contact analysis separately in the same manner. After performing the contact analysis of the cylinder with each type of diseased artery, the contact normal forces on the cylinder imposed by the vessel in each case were applied as loads on the same cylindrical stent design domain, for optimisation.

2.3 Topology Optimisation

The next step was to perform the topology optimisation. Topology optimisation can provide an optimised "design concept" of materials distribution, potentially achieving greater design improvement than size and shape optimisation [49]. In this case the aim was to achieve a stent design concept to best suit lesion-specific conditions. The objective was to minimise the compliance C^* of the structure (where C^* is the reciprocal of stiffness) while satisfying the constraints of volume fraction (while being in the range of current stents in practice in terms of stent-artery area coverage ratio) under contact loading conditions of the stenotic artery. The compliance of a structure is defined as

$$C^* = \boldsymbol{U}^T \boldsymbol{F} \qquad (2)$$

where $\boldsymbol{U}$ is the global displacement vector and $\boldsymbol{F}$ is the global force vector applied to the structure. The strain energy *S* of the structure is defined as

$$S = \frac{1}{2}\boldsymbol{U}^T\boldsymbol{F} \tag{3}$$

Assuming constant $\boldsymbol{F}$, minimising compliance would mean minimising strain energy or the deformation $\boldsymbol{U}$, in an elastic regime. The density method or the solid isotropic material with penalisation (SIMP) method was applied for stent topology optimisation [50–52] using MSC Nastran. The SIMP method assigns an internal element density x^i to each element, which is the design variable of the optimisation.

The SIMP method then minimises compliance as follows

Objective: $$\min C^* = \boldsymbol{U}^T\boldsymbol{F} \tag{4}$$

$$C^* = \boldsymbol{U}^T\boldsymbol{K}\boldsymbol{U} = \sum_{i=1}^{N} u^i k^i u^i$$

$$= \sum_{i=1}^{N} (x^i)^p u^i k_0 u^i$$

Subject to volume constraint: $$V = \sum_{i=1}^{N} x^i v^i \leq V_0 - V^* \tag{5}$$

$$\boldsymbol{F} = \boldsymbol{K}\boldsymbol{U}$$

$$k^i = (x^i)^p \, k_0$$

$$0 < x_{min} \leq x^i \leq x_{max} < 1$$

where $\boldsymbol{K}$ is the stiffness matrix of the stent structure, u^i is the displacement vector of the nodes, N is the total number of elements, k_0 and k^i are the element's initial stiffness and the stiffness matrix after optimisation, respectively.

In the constraints, V is the volume of the structure after optimisation which in our case was set to 0.3 (30%) based on being in the range (25%-65%) of currently available polymer

stents [53]. V_0 is the initial volume, V^* the amount of material to be removed, v^i is the element volume after optimisation.

The density design variable x^i of each element has a value ranging between 0 (void) and 1 (solid). Elements with values close to 0 can be discarded, since they represent regions where little stress is being carried, whilst those nearest to 1 are bearing the largest load. x_{min} is the lower bound of element density and x_{max} is the upper bound of element density. The reason for keeping a lower bound for the density instead of restricting it to zero is to avoid singularity of the system's matrices. A penalty factor *p* is introduced to enforce the design variable to be close to 0-1 solution when *p*>1.0 [42]. A recommended value of 3 is used for this problem, this approach is simple and the optimised design consists of clear solid and void without the undue suppression of local optima.

2.4 Comparison with a Generic Stent

The main aim of stent implantation is to keep the artery open by pushing the plaque against the arterial wall. Therefore a stent should have enough radial stiffness to deal with different types of plaques in terms of their shape and stiffness. In this study a set of plaque types with different size and stiffness have been used, hence focus is kept on the stent performance in terms of radial recoil after implantation. After performing contact analysis of the new optimised stents with their respective stenotic artery types, the final step of the study was to simulate a typical generic stent in similar fashion and compare its radial deformation to the topologically optimised stents. The generic stent used was expanded with the help of internal pressure of 0.52 MPa such that it plastically deformed to its final diameter of 5.15 mm inside corresponding arteries.

3 RESULTS & DISCUSSION

As described above, the initial contact analyses involving the artery models with the cylinder were used to generate a set of contact normal forces acting radially inward on the cylinder for each case, to be used as the input load for the topology optimisation. An example of the resultant radial force from a contact analysis is shown in Figure 7. This Figure depicts the contour plot of the radially inward nodal forces on the cylinder. It could be noted in Fig. 7b that highest load is acting on the top centre due to peak plaque thickness (results of axial-stent-half unwrapped from cylindrical shape for illustration purpose).

Topology optimisation using the force distribution from the contact analysis was used to generate the optimal material distribution of material for the 9 different plaque loading conditions. Figure 8 shows the normalised material density distribution, from TO with a 0.3 volume fraction constraint. The resulting amount of material in each optimised stent was similar to the generic stent (varying less than 5%). The results were unwrapped using MATLAB to form a flat 2-D plot for illustration purposes. It can be seen that there is a higher material density in the central part of the stent, as a consequence of the plaque induced higher forces here as previously shown in Figure 7, especially in the centre of the lower half of each stent where it comes into contact with the thickest part of the plaque in each case.

Matlab and image editing software were used to unwrap, construct and smooth the optimisation geometry in order to transform it into an analysable stent structure, as illustrated in Figure 9. This modification lead to an additional 5-10% volume increase of

the stent but the overall volume remained in the range of current stents in practice. The smoothed optimised stent results were then wrapped to form cylindrical shapes and solved for contact analysis with their respective arteries in the same manner as the contact FEA with the force extracting cylinder. The final lumen radial deformation of 20 equidistant points in each of the diseased arteries along the thickest part of plaque were recorded to provide a comparative measure of the ability of the stent to maintain arterial opening.

For comparison, the first step was to evaluate recoil of generic stent in unstenotic and stenotic arteries with different plaque materials for 30, 40 and 50% stenosis levels respectively as shown in Figure 10a-10c. Plaque peak thickness in the 30% stenosis protruding inside the artery had a minimum unstented radius 1.56 mm, as shown in Figure 10d. After implantation of optimised stents, this increased to 2.43 mm, 2.54 mm and 2.54 mm for calcified, cellular and hypocellular plaques respectively with the corresponding optimised stent. In the same scenario, lumen position values after generic stent implantation were 2.17 mm, 2.29 mm and 2.24 mm for calcified, cellular and hypocellular plaques respectively. In the 40% stenotic artery, the unstented minimum position from central axis was, as expected, even less than with the 30% plaque, at 1.22mm. After stenting with the optimised designs, lumen gain was achieved, with the minimum radius increasing to 2.24 mm, 2.51 mm and 2.34 mm for calcified, cellular and hypocellular plaques respectively, with the corresponding optimised stent as illustrated in Figure 10e. Results in the same environment with generic stent were 1.68 mm, 2.13 mm and 2.0 mm for calcified, cellular and hypocellular plaques respectively. Similarly for 50% artery

stenosis, plaque peak thickness had an unstented position of 0.972 mm in the Z direction. After stenting this increased to 2.06 mm, 2.49 mm and 2.50 mm for calcified, cellular and hypocellular respectively, with the corresponding optimised stent (Figure 10f). In similar conditions, lumen positions with a generic stent were 1.54 mm, 1.97 mm and 1.78 mm for calcified, cellular and hypocellular plaques respectively.

Analysis of the generic stent studied shows that severe calcification could lead to immediate lumen gain after the implantation of self-expanding stents as illustrated in Figure 10,11. The generic stent deployed in the calcified 30%, 40% and 50% diseased vessel, recoiled significantly more than the optimised stents in the central region leading to 10%, 29% and 35% residual stenosis respectively (Figure 10a-10c & 11). This was in agreement with a previous study mentioned earlier [4]. In other words, in spite of having similar volume of material, the stent showed less efficacy in supporting the disease and the displacement could not meet the limits of standard stenting effectiveness of 30% or lower allowable immediate post-implantation residual stenosis [11,12].

These results reveal the potential of the proposed design method, utilising contact FEA and topology optimisation, to generate optimised stents able to restore the lumen area to an acceptable level for given plaque types, i.e. resulting recoil lower than 30% residual stenosis, whilst retaining beneficial features, such as lower stent volume. It could be noted that the calcified lesion, owing to its greater stiffness, leads to slightly lower stented lumen area compared to the other plaque types in all types of stenosis; optimised stent performance post stenting is still acceptable. The proposed method also has the potential

to eliminate the need for balloon angioplasty and related procedures, which are commonly performed to create a more uniform lesion to be stented [54].

The results obtained from the topology optimisation give a concept design and demonstrate that stents could be tailored according to the accurate loading conditions in specific-plaques geometries. Topology optimisation results are normally mesh-dependent and therefore could be further investigated by employing different methods to refine the desired solution. One such recently developed method [33] is the use of extended finite element method (X-FEM), in combination with an evolutionary optimisation method that allows to obtain smooth and clearly defined structural boundaries and would potentially reduce the need to modify the TO results to obtain a manufacturable design.

4 LIMITATIONS AND FUTURE WORK

The current work does not consider stent crimping and expansion process in the design approach and is focused on early-stage topology optimisation to achieve geometries at a conceptual stage. A complete, but challenging solution is to use a topology optimisation method to create a compliant mechanism [55] and simulate implantation. However, one is not always dependent on plastic deformation to fix a stent, for example, another one potential route is to incorporate a ratchet-like mechanism to the designs similar to the REVA stent and a recoil prevention device [53,56,57], which upon balloon expansion has struts that slide and lock without plastic deformation of the stent. In the future, a more complete study will involve the examination of curved and bifurcating systems, as well as

the importance of advanced material models including anisotropic, plastic and failure modes [58,59]. Further studies should also consider other materials such as stronger bioresorbable polymers and biocompatible super-elastic alloys such as nitinol.

This approach to design of stents will likely realise complex topographies that will be difficult to manufacture with traditional techniques. Whilst these could be manufactured using, for example, laser cutting methods common for stent production, a technology for the future is additive manufacturing (AM). Production and modification of metallic stents via AM has already been demonstrated and printable polymeric biomaterials for drug release and implants are becoming more widely available [60–67]. The workflow presented here has potential benefit not only for the personalised treatment of CVD; the scalability and freedom of design based AM offers a benefit for other intravascular applications. The combination of design, additive manufacturing and identification of patient specific arterial geometries and properties offers considerable patient benefit.

5 CONCLUSION

A topology optimisation method has been applied to the optimisation of stent geometry for a set of specific lesion sizes and types. After transforming the TO results to manufacturable design concepts, it has been demonstrated that such designs are able to maintain lumen area to a greater degree than a selected generic design. Through mechanical design the stent recoil was reduced, even under conditions of significant stenosis and strong variations in the material solid rheology.

ACKNOWLEDGMENT

This work was funded by the University of Nottingham, as part of the EPSRC Centre for Innovative Manufacturing in Additive Manufacturing, grant reference EP/I033335/2 and by Loughborough University.

NOMENCLATURE

E	elastic modulus
v	Poisson's ratio
σ_y	yield stress
W	strain energy density function
C	hyperelastic constants
I	strain invariants
C^*	compliance
$\boldsymbol{U}$	global displacement vector
$\boldsymbol{F}$	global force vector
S	strain energy
$\boldsymbol{K}$	stiffness matrix
N	total number of elements
u^i	displacement vector of the nodes

k^i	stiffness matrix after optimisation
k_0	elements initial stiffness
x^i	initial element density
V_0	initial volume
V	volume of the structure after optimisation
V^*	amount of material to be removed
v^i	element volume after optimisation
x_{min}	lower bound of element density
x_{max}	upper bound of element density
p	penalty factor

REFERENCES

[1] National Health Service UK, "Cardiovascular disease", accessed March 27, 2013, http://www.nhs.uk/conditions/cardiovascular-disease/Pages/Introduction.aspx.

[2] Sigwart, U., Puel, J., Mirkovitch, V., Joffre, F., and Kappenberger, L., 1987, "Intravascular stents to prevent occlusion and restenosis after transluminal angioplasty," N. Engl. J. Med., **316**(12), pp. 701–6.

[3] McClean, D. R., Eiger, N. L., and Eigler, N. L., 2001, "Stent Design : Implications for Restenosis," Rev. Cardiovasc. Med., **3**, pp. S16–22.

[4] Hara, H., Nakamura, M., Palmaz, J. C., and Schwartz, R. S., 2006, "Role of stent design and coatings on restenosis and thrombosis," Adv. Drug Deliv. Rev., **58**(3), pp. 377–86.

[5] Poncin, P., and Proft, J., 2003, "Stent Tubing : Understanding the Desired Attributes," Medical Device Materials: Proceedings of the Materials & Processes for Medical Devices Conference. Materials Park, OH: ASM International, pp. 253–259.

[6] Morton, A. C., Crossman, D., and Gunn, J., 2004, "The influence of physical stent parameters upon restenosis," Pathol. Biol. (Paris)., **52**(4), pp. 196–205.

[7] Rogers, C., and Edelman, E. R., 1995, "Endovascular stent design dictates experimental restenosis and thrombosis," Circulation, (91), pp. 2995–3001.

[8] Kastrati, A., Mehilli, J., Dirschinger, J., Pache, J., Ulm, K., Schühlen, H., Seyfarth, M., Schmitt, C., Blasini, R., Neumann, F. J., and Schömig, A., 2001, "Restenosis after coronary placement of various stent types," Am. J. Cardiol., **87**(1), pp. 34–9.

[9] Lee, R. T., Grodzinsky, A. J., Frank, E. H., Kamm, R. D., and Schoen, F. J., 1991, "Structure-dependent dynamic mechanical behavior of fibrous caps from human atherosclerotic plaques," Circulation, **83**(5), pp. 1764–1770.

[10] Zhao, S., Gu, L., and Froemming, S. R., 2012, "Finite Element Analysis of the Implantation of a Self-Expanding Stent: Impact of Lesion Calcification," ASME J. Med. Devices, **6**(2), p. 021001.

[11] Elezi, S., Kastrati, a., Neumann, F.-J., Hadamitzky, M., Dirschinger, J., and Schomig, a., 1998, "Vessel Size and Long-Term Outcome After Coronary Stent Placement," Circulation, **98**(18), pp. 1875–1880.

[12] Krankenberg, H., Schlüter, M., Steinkamp, H. J., Bürgelin, K., Scheinert, D., Schulte, K.-L., Minar, E., Peeters, P., Bosiers, M., Tepe, G., Reimers, B., Mahler, F., Tübler, T., and Zeller, T., 2007, "Nitinol stent implantation versus percutaneous transluminal angioplasty in superficial femoral artery lesions up to 10 cm in length: the femoral artery stenting trial (FAST)," Circulation, **116**(3), pp. 285–92.

[13] García, A., Peña, E., and Martínez, M. A., 2012, "Influence of geometrical parameters on radial force during self-expanding stent deployment. Application for a variable radial stiffness stent," J. Mech. Behav. Biomed. Mater., **10**, pp. 166–75.

[14] Pericevic, I., Lally, C., Toner, D., and Kelly, D. J., 2009, "The influence of plaque composition on underlying arterial wall stress during stent expansion: the case for lesion-specific stents," Med. Eng. Phys., **31**(4), pp. 428–33.

[15] Nissen, S. E., and Yock, P., 2001, "Intravascular Ultrasound: Novel Pathophysiological Insights and Current Clinical Applications," Circulation, **103**(4), pp. 604–616.

[16] Budoff, M. J., Achenbach, S., Blumenthal, R. S., Carr, J. J., Goldin, J. G., Greenland, P., Guerci, A. D., Lima, J. A. C., Rader, D. J., Rubin, G. D., Shaw, L. J., and Wiegers, S. E., 2006, "Assessment of coronary artery disease by cardiac computed tomography," Circulation, **114**(16), pp. 1761–91.

[17] Dweck, M. R., Puntmann, V. O., Vesey, A. T., Fayad, Z. A., and Nagel, E., 2016, "MR Imaging of Coronary Arteries and Plaques," JACC Cardiovasc. Imaging, **9**(3), pp. 306–316.

[18] Makowski, M. R., Henningsson, M., Spuentrup, E., Kim, W. Y., Maintz, D., Manning, W. J., and Botnar, R. M., 2013, "Characterization of Coronary Atherosclerosis by Magnetic Resonance Imaging," Circulation, **128**(11), pp. 1244–1255.

[19] Huang, D., Swanson, E. A., Lin, C. P., Schuman, J. S., Stinson, W. G., Chang, W., Hee, M. R., Flotte, T., Gregory, K., Puliafito, C. A., and Fujimoto, J. G., 1991, "Optical Coherence Tomography," Science, **254**(5035), pp. 1178–1181.

[20] Kim, D.-H., Lu, N., Ghaffari, R., Kim, Y.-S., Lee, S. P., Xu, L., Wu, J., Kim, R.-H., Song, J., Liu, Z., Viventi, J., de Graff, B., Elolampi, B., Mansour, M., Slepian, M. J., Hwang, S., Moss, J. D., Won, S.-M., Huang, Y., Litt, B., and Rogers, J. A., 2011, "Materials for multifunctional balloon catheters with capabilities in cardiac electrophysiological mapping and ablation therapy," Nat Mater, **10**(4), pp. 316–323.

[21] Slepian, M. J., Ghaffari, R., and Rogers, J. A., 2011, “Multifunctional balloon catheters of the future,” Interv. Cardiol., **3**(4), pp. 417–419.

[22] Iqbal, J., Onuma, Y., Ormiston, J., Abizaid, A., Waksman, R., and Serruys, P., 2014, “Bioresorbable scaffolds: rationale, current status, challenges, and future,” Eur. Heart J., **35**(12), pp. 765–76.

[23] Moore, J. E., Soares, J. S., and Rajagopal, K. R., 2010, “Biodegradable Stents: Biomechanical Modeling Challenges and Opportunities,” Cardiovasc. Eng. Technol., **1**(1), pp. 52–65.

[24] Huang, X., and Xie, Y. M., 2010, Evolutionary topology optimization of continuum structures: methods and applications, Wiley, Chichester.

[25] Bendsøe, M. P., and Kikuchi, N., 1988, “Generating optimal topologies in structural design using a homogenization method,” Comput. Methods Appl. Mech. Eng., **71**(2), pp. 197–224.

[26] Bendsøe, M. P., 1989, “Optimal shape design as a material distribution problem,” Struct. Optim., **1**(4), pp. 193–202.

[27] Zhou, M., and Rozvany, G. I. N., 1991, “The COC algorithm, Part II: Topological, geometrical and generalized shape optimization,” Comput. Methods Appl. Mech. Eng., **89**(1-3), pp. 309–336.

[28] Wang, M. Y., Wang, X., and Guo, D., 2003, “A level set method for structural topology optimization,” Comput. Methods Appl. Mech. Eng., **192**(1-2), pp. 227–246.

[29] Allaire, G., Jouve, F., and Toader, A.-M., 2004, “Structural optimization using sensitivity analysis and a level-set method,” J. Comput. Phys., **194**(1), pp. 363–393.

[30] Xie, Y. M., and Steven, G. P., 1993, “A simple evolutionary procedure for structural optimization,” Comput. Struct., **49**(5), pp. 885–896.

[31] Querin, O. M., Steven, G. P., and Xie, Y. M., 1998, “Evolutionary structural optimisation (ESO) using a bidirectional algorithm,” Eng. Comput., **15**(8), pp. 1031–1048.

[32] Yang, X. Y., Xei, Y. M., Steven, G. P., and Querin, O. M., 1999, “Bidirectional Evolutionary Method for Stiffness Optimization,” AIAA J., **37**(11), pp. 1483–1488.

[33] Abdi, M., Wildman, R., and Ashcroft, I., 2013, “Evolutionary topology optimization using the extended finite element method and isolines,” Eng. Optim., **46**(5), pp. 628–647.

[34] Bedoya, J., Meyer, C. a, Timmins, L. H., Moreno, M. R., and Moore, J. E., 2006, “Effects of stent design parameters on normal artery wall mechanics,” ASME J. Biomech. Eng., **128**(5), pp. 757–65.

[35] Migliavacca, F., Petrini, L., Montanari, V., Quagliana, I., Auricchio, F., and Dubini, G., 2005, “A predictive study of the mechanical behaviour of coronary stents by computer modelling,” Med. Eng. Phys., (27), pp. 13–18.

[36] Etave, F., Finet, G., Boivin, M., Boyer, J. C., Rioufol, G., and Thollet, G., 2001, “Mechanical properties of coronary stents determined by using finite element analysis,” J. Biomech., **34**(8), pp. 1065–75.

[37] Petrini, L., Migliavacca, F., Auricchio, F., and Dubini, G., 2004, “Numerical investigation of the intravascular coronary stent flexibility,” J. Biomech., **37**(4), pp. 495–501.

[38] Timmins, L. H., Meyer, C. a, Moreno, M. R., and Moore, J. E., 2008, “Effects of stent design and atherosclerotic plaque composition on arterial wall biomechanics,” J. Endovasc. Ther., **15**(6), pp. 643–54.

[39] Wu, W., Yang, D.-Z., Huang, Y.-Y., Qi, M., and Wang, W.-Q., 2008, “Topology optimization of a novel stent platform with drug reservoirs,” Med. Eng. Phys., **30**(9), pp. 1177–85.

[40] Guimarães, T. a., Oliveira, S. a. G., and Duarte, M. a., 2008, “Application of the topological optimization technique to the stents cells design for angioplasty,” J. Brazilian Soc. Mech. Sci. Eng., **30**(3), pp. 261–268.

[41] Liu, Q., 2014, “Concept Design of Cardiovascular Stents Based on Load Identification,” J. Inst. Eng. Ser. C, **96**(2), pp. 99–105.

[42] Bendsøe, M. P., and Sigmund, O., 1999, “Material interpolation schemes in topology optimization,” Arch. Appl. Mech., **69**(9-10), pp. 635–654.

[43] Van Andel, C. J., Pistecky, P. V, and Borst, C., 2003, “Mechanical properties of porcine and human arteries: implications for coronary anastomotic connectors,” Ann. Thorac. Surg., **76**(1), pp. 58–64; discussion 64–65.

[44] Tamai, H., Igaki, K., Tsuji, T., Kyo, E., Kosuga, K., Kawashima, A., Matsui, S., Komori, H., Motohara, S., Uehata, H., and Takeuchi, E., 1999, “A Biodegradable

Poly-l-lactic Acid Coronary Stent in the Porcine Coronary Artery," J. Interv. Cardiol., **12**(6), pp. 443–450.

[45] Jamshidian, M., Tehrany, E. A., Imran, M., Jacquot, M., and Desobry, S., 2010, "Poly-Lactic Acid: Production, Applications, Nanocomposites, and Release Studies," Compr. Rev. Food Sci. Food Saf., **9**(5), pp. 552–571.

[46] Vroman, I., and Tighzert, L., 2009, "Biodegradable polymers," Materials (Basel)., **2**(2), pp. 307–344.

[47] Nishida, M., Yamaguchi, M., Todo, M., Takayama, T., Häggblad, H.-Å., and Jonsén, P., 2009, "Evaluation of dynamic compressive properties of PLA polymer blends using split Hopkinson pressure bar," DYMAT 2009 - 9th International Conferences on the Mechanical and Physical Behaviour of Materials under Dynamic Loading, Brussels, Belgium, pp. 909–915.

[48] Lally, C., Reid, A. J., and Prendergast, P. J., 2004, "Elastic Behavior of Porcine Coronary Artery Tissue Under Uniaxial and Equibiaxial Tension," Ann. Biomed. Eng., **32**(10), pp. 1355–1364.

[49] Sigmund, O., 2000, "Topology optimization: a tool for the tailoring of structures and materials," Philos. Trans. R. Soc. A Math. Phys. Eng. Sci., **358**(1765), pp. 211–227.

[50] Bendsoe, M., and Sigmund, O., 1999, "Material interpolation schemes in topology optimization," Arch Appl Mech, (69), pp. 635–54.

[51] Kiziltas, G., Kikuchi, N., Volakis, J., and Halloran, J., 2004, "Topology optimization of dielectric substrates for filters and antennas using SIMP," Arch Comput Methods Eng, (11), pp. 355–88.

[52] Zuo, K., Chen, L., Zhang, Y., and Yang, J., 2007, "Study of key algorithms in topology optimization," Int J Adv Manufact Technol, (32), pp. 787– 96.

[53] Ormiston, J. A., and Serruys, P. W. S., 2009, "Bioabsorbable coronary stents," Circulation, **2**(3), pp. 255–60.

[54] Martinez-Elbal, L., Ruiz-Nodar, J. M., Zueco, J., Lopez-Minguez, J. R., Moreu, J., Calvo, I., Ramirez, J. A., Alonso, M., Vazquez, N., Lezaun, R., and Rodriguez, C., 2002, "Direct coronary stenting versus stenting with balloon pre-dilation: immediate and follow-up results of a multicentre, prospective, randomized study. The DISCO trial. DIrect Stenting of COronary Arteries," Eur. Heart J., **23**(8), pp. 633–640.

[55] Yin, L., and Ananthasuresh, G. K., 2001, “Topology optimization of compliant mechanisms with multiple materials using a peak function material interpolation scheme,” Struct. Multidiscip. Optim., **23**(1), pp. 49–62.

[56] Ramcharitar, S., and Serruys, P., 2008, “Fully Biodegradable Coronary Stents,” Am. J. Cardiovasc. Drugs, **8**(5), pp. 305–314.

[57] Mehdizadeh, A., Ali, M. S. M., Takahata, K., Al-Sarawi, S., and Abbott, D., 2013, “A recoil resilient lumen support, design, fabrication and mechanical evaluation,” J. Micromechanics Microengineering, **23**(6), p. 065001.

[58] Gamero, L. G., Armentano, R. L., and Levenson, J., 2002, “Arterial wall diameter and viscoelasticity variability,” IEEE Computers in Cardiology, Memphis, Tennessee, USA, pp. 513–516.

[59] Moore, J. J., and Berry, J. L., 2002, “Fluid and solid mechanical implications of vascular stenting,” Ann. Biomed. Eng., **30**(4), pp. 498–508.

[60] Vaithilingam, J., Kilsby, S., Goodridge, R. D., Christie, S. D. R., Edmondson, S., and Hague, R. J. M., 2015, “Functionalisation of Ti6Al4V components fabricated using selective laser melting with a bioactive compound,” Mater. Sci. Eng. C, **46**, pp. 52–61.

[61] Vaithilingam, J., Kilsby, S., Goodridge, R. D., Christie, S. D. R., Edmondson, S., and Hague, R. J. M., 2014, “Immobilisation of an antibacterial drug to Ti6Al4V components fabricated using selective laser melting,” Appl. Surf. Sci., **314**, pp. 642–654.

[62] He, Y., Wildman, R. D., Tuck, C. J., Christie, S. D. R., and Edmondson, S., 2016, “An Investigation of the Behavior of Solvent based Polycaprolactone ink for Material Jetting,” Sci. Rep., **6**, p. 20852.

[63] Gunasekera, D. H. A. T., Kuek, S., Hasanaj, D., He, Y., Tuck, C., Croft, A., and Wildman, R. D., 2016, “Three dimensional ink-jet printing of biomaterials using ionic liquids and co-solvents,” Faraday Discuss., **190**, pp. 509–523.

[64] He, Y., Tuck, C. J., Prina, E., Kilsby, S., Christie, S. D. R., Edmondson, S., Hague, R. J. M., Rose, F. R. A. J., and Wildman, R. D., 2016, “A new photocrosslinkable polycaprolactone-based ink for three-dimensional inkjet printing.,” J. Biomed. Mater. Res. B. Appl. Biomater., 00B(00).

[65] Begines, B., Hook, A. L., Alexander, M. R., Tuck, C. J., and Wildman, R. D., 2016, “Development, printability and post-curing studies of formulations of materials

resistant to microbial attachment for use in inkjet based 3D printing," Rapid Prototyp. J., 22(5), pp. 835–841.

[66] Seyednejad, H., Gawlitta, D., Dhert, W. J. A., van Nostrum, C. F., Vermonden, T., and Hennink, W. E., 2011, "Preparation and characterization of a three-dimensional printed scaffold based on a functionalized polyester for bone tissue engineering applications," Acta Biomater., **7**(5), pp. 1999–2006.

[67] Williams, J. M., Adewunmi, A., Schek, R. M., Flanagan, C. L., Krebsbach, P. H., Feinberg, S. E., Hollister, S. J., and Das, S., 2005, "Bone tissue engineering using polycaprolactone scaffolds fabricated via selective laser sintering," Biomaterials, **26**(23), pp. 4817–4827.

Table Caption List

Table 1 Hyperelastic constants to describe plaque and arterial tissue [48].

Figure Captions List

Fig. 1 Analysis steps.

Fig. 2 Proposed approach to design lesion-specific stents.

Fig. 3 Artery models with plaque types used for the analyses (XZ plane cut view).

Fig. 4 Generic stent used for comparison.

Fig. 5 Maximum radial displacement of plaque tip in the artery with five different meshes.

Fig. 6 Relative position of cylinder and 40% stenotic artery before contact (artery sliced for illustration purpose).

Fig. 7 Contour plot showing radially inward nodal load (N) variation on one of the 9 design spaces for stent topology optimisation based on cylinder-artery contact with 50% calcified stenosis (a), discrete load contour plot unwrapped from cylindrical shape for illustration purpose showing axial (X) and circumferential (Θ) directions (b).

Fig. 8 Stent topology optimisation density distribution results for (a-c) 30%, (d-f) 40% and (g-i) 50% stenosis for calcified, cellular and hypocellular plaque types respectively (results of axial-stent-half unwrapped from cylindrical shape for illustration purpose).

Fig. 9 Stent topologies for (a-c) 30%, (d-f) 40% and (g-i) 50% for calcified, cellular and hypocellular plaque types respectivelys, (results of axial-stent-half unwrapped from cylindrical shape for illustration purpose).

Fig. 10 Final lumen radial deformation with a generic stent (a-c) and optimised stents (d-f) for 30, 40 and 50% stenotic arteries respectively with different plaque types based on 11 equally distant points longitudinally along thickest part of plaque, relative to central axis (one half of the stenotic artery deformations illustrated).

Fig. 11 Post implantation stenosis levels (calculated by lesion cross-sectional area) in the remodeled artery due to optimised and generic stents recoil.

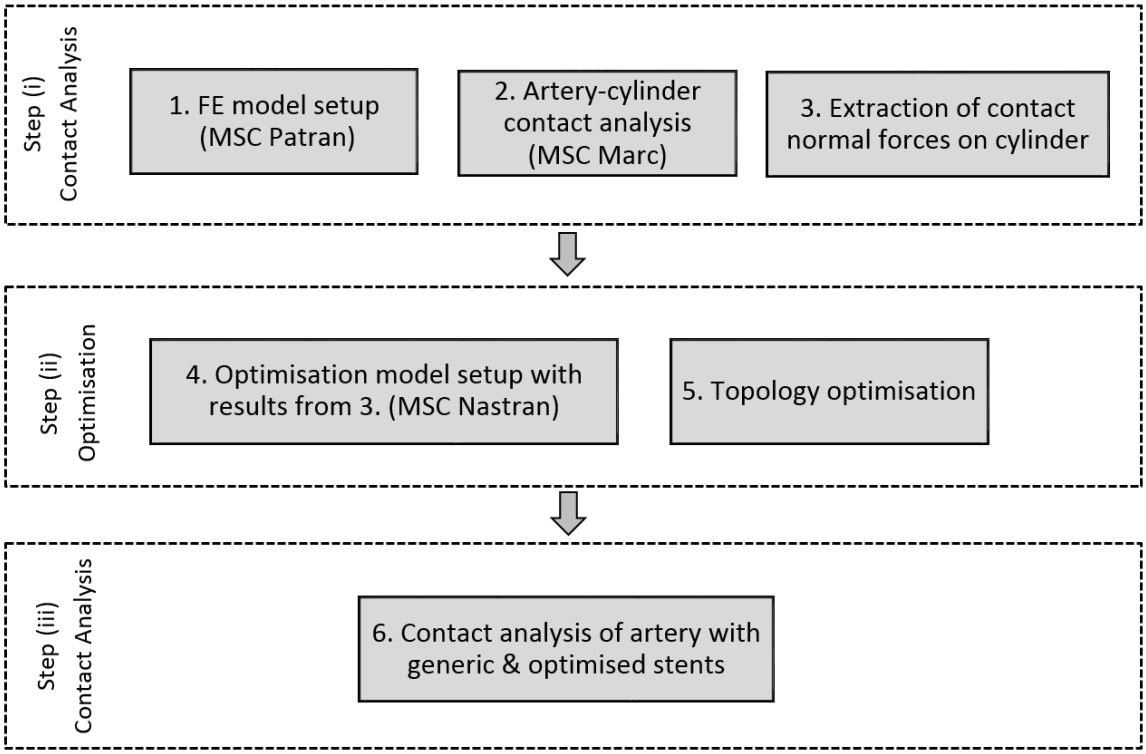

Figure 1

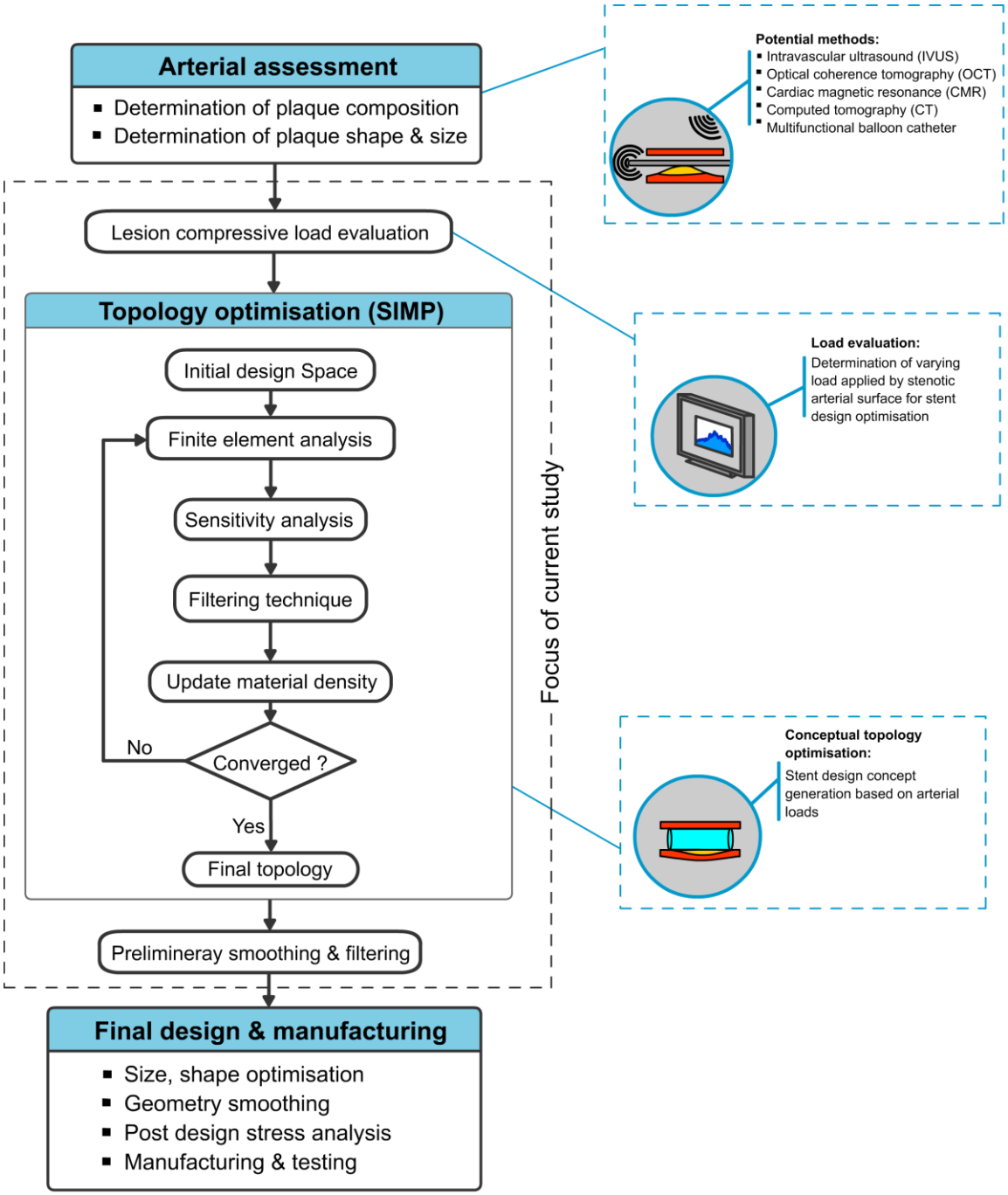

Figure 2

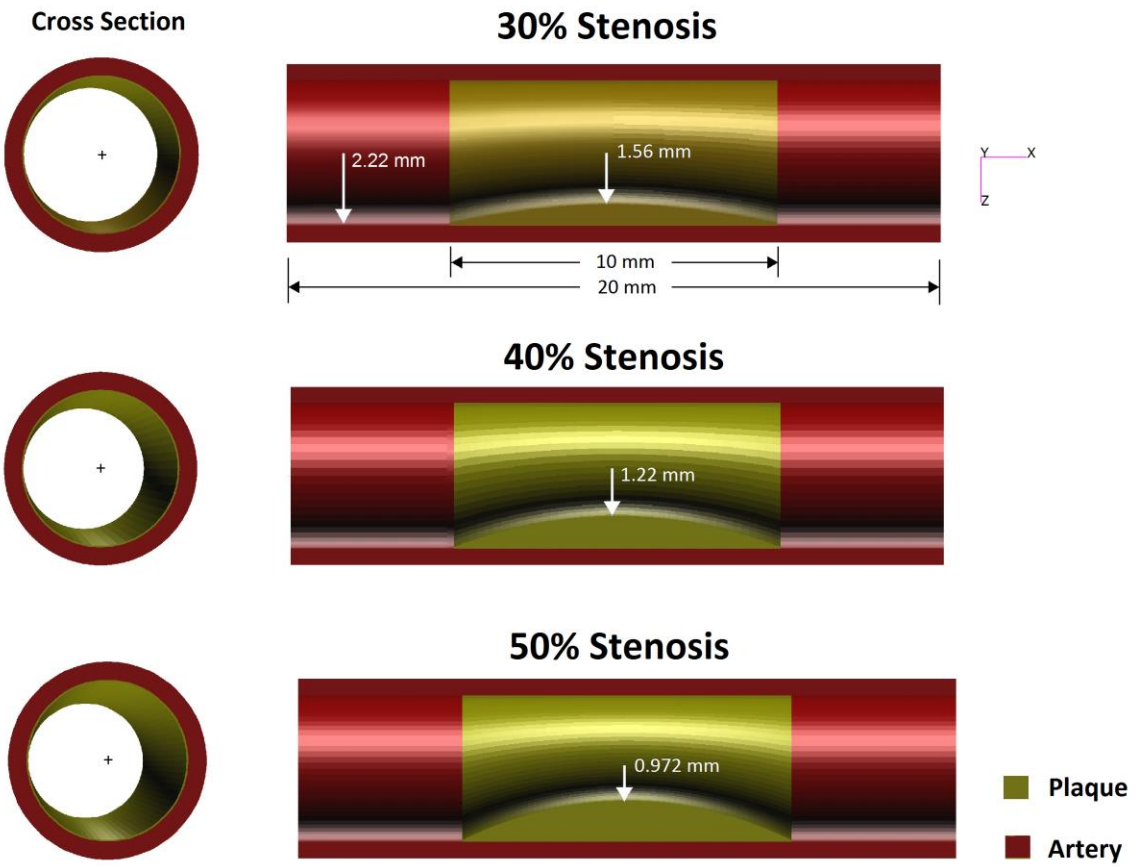

Figure 3

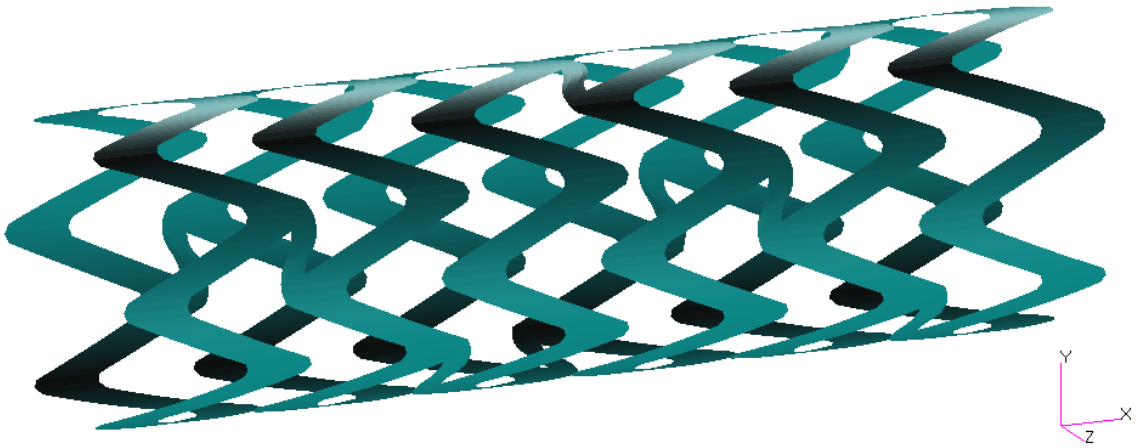

Figure 4

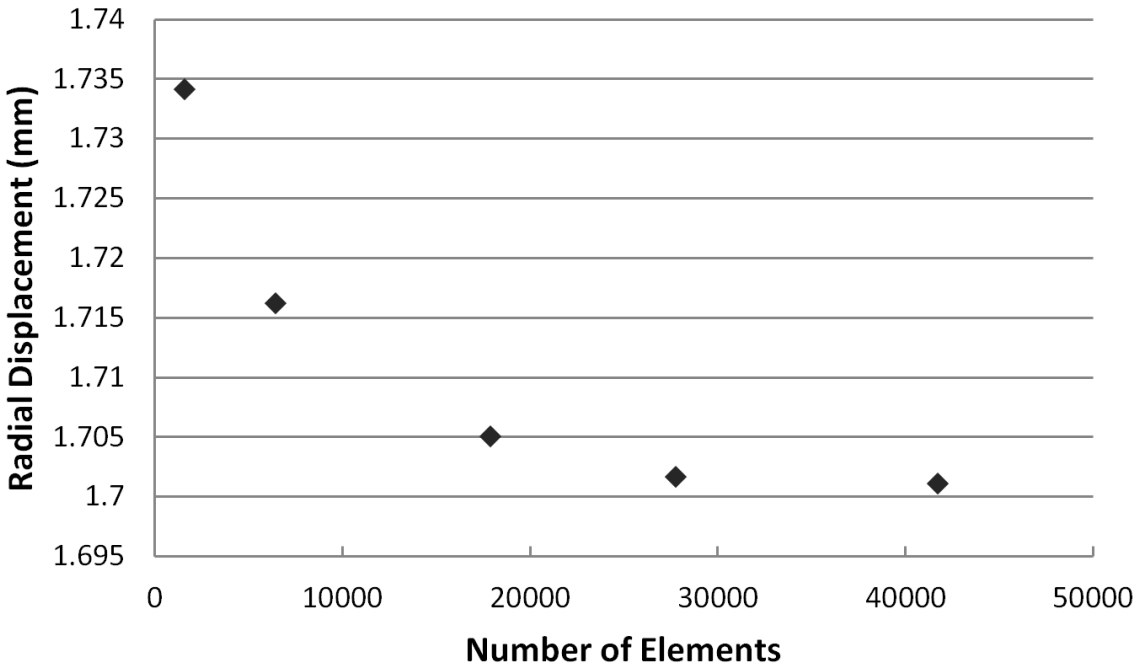

Figure 5

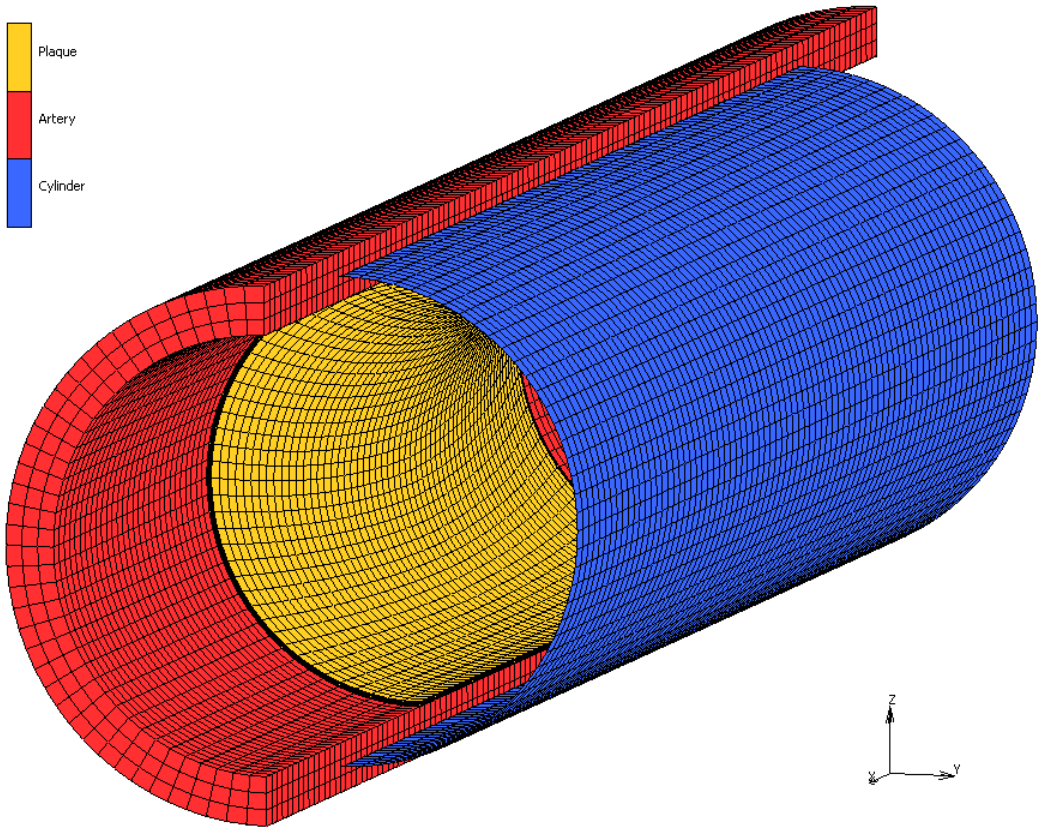

Figure 6

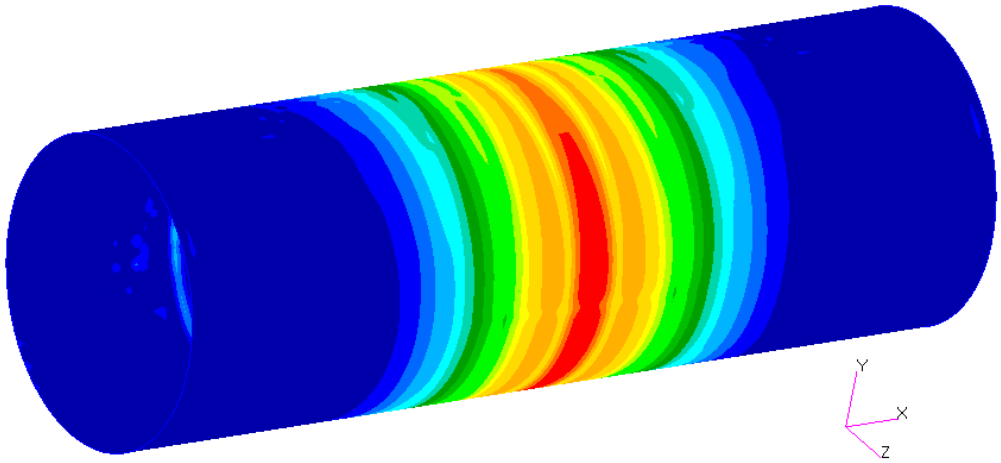

(a)

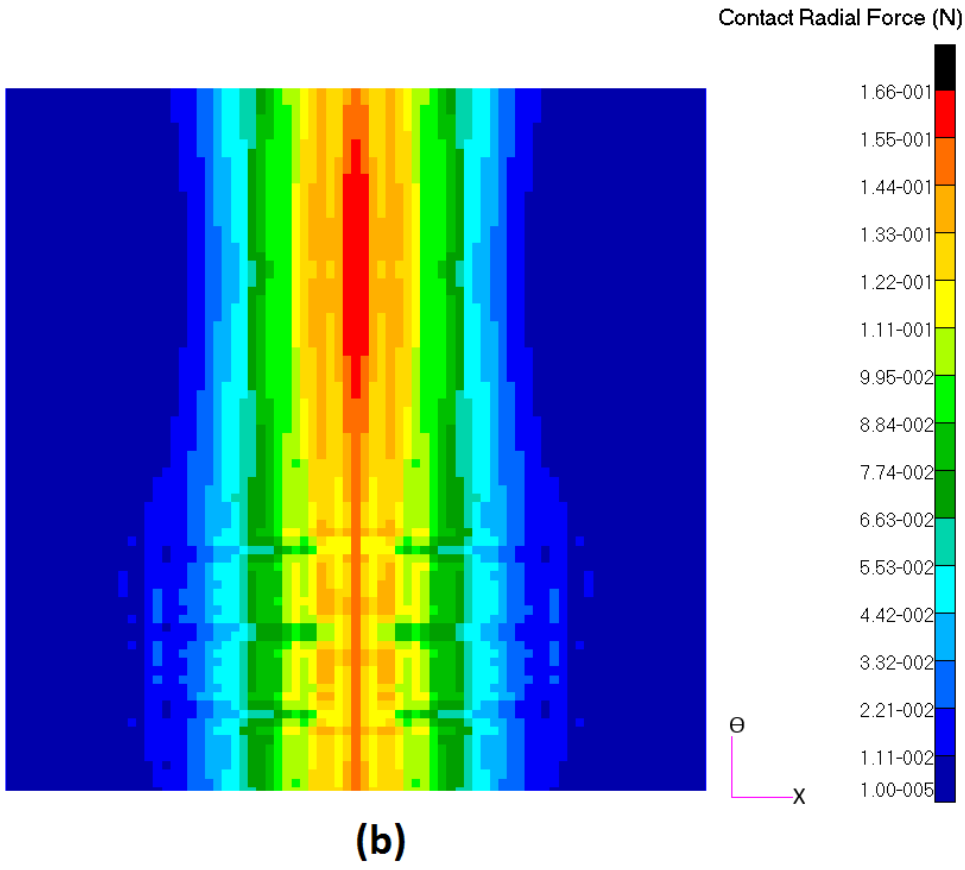

(b)

Figure 7

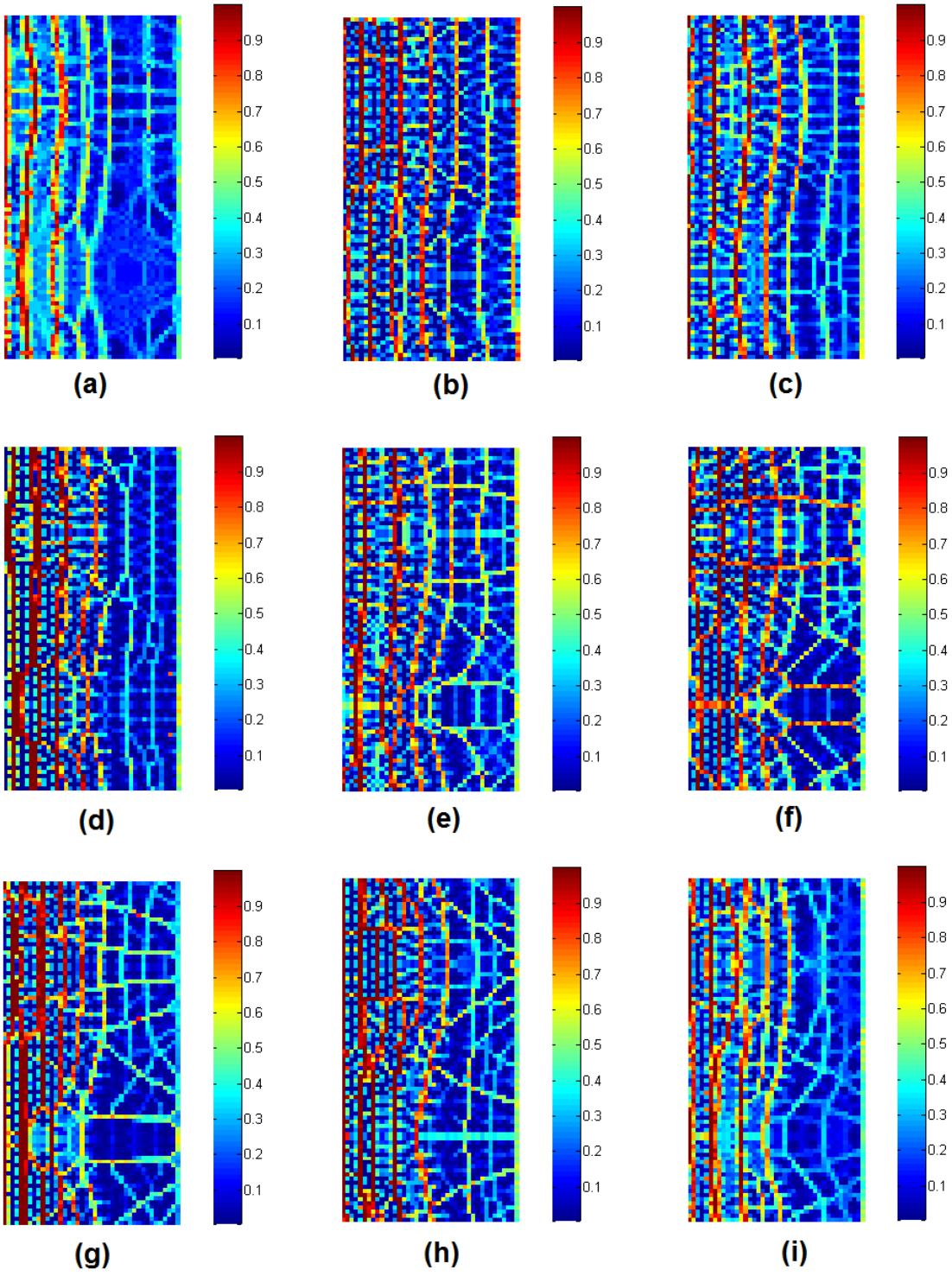

Figure 8

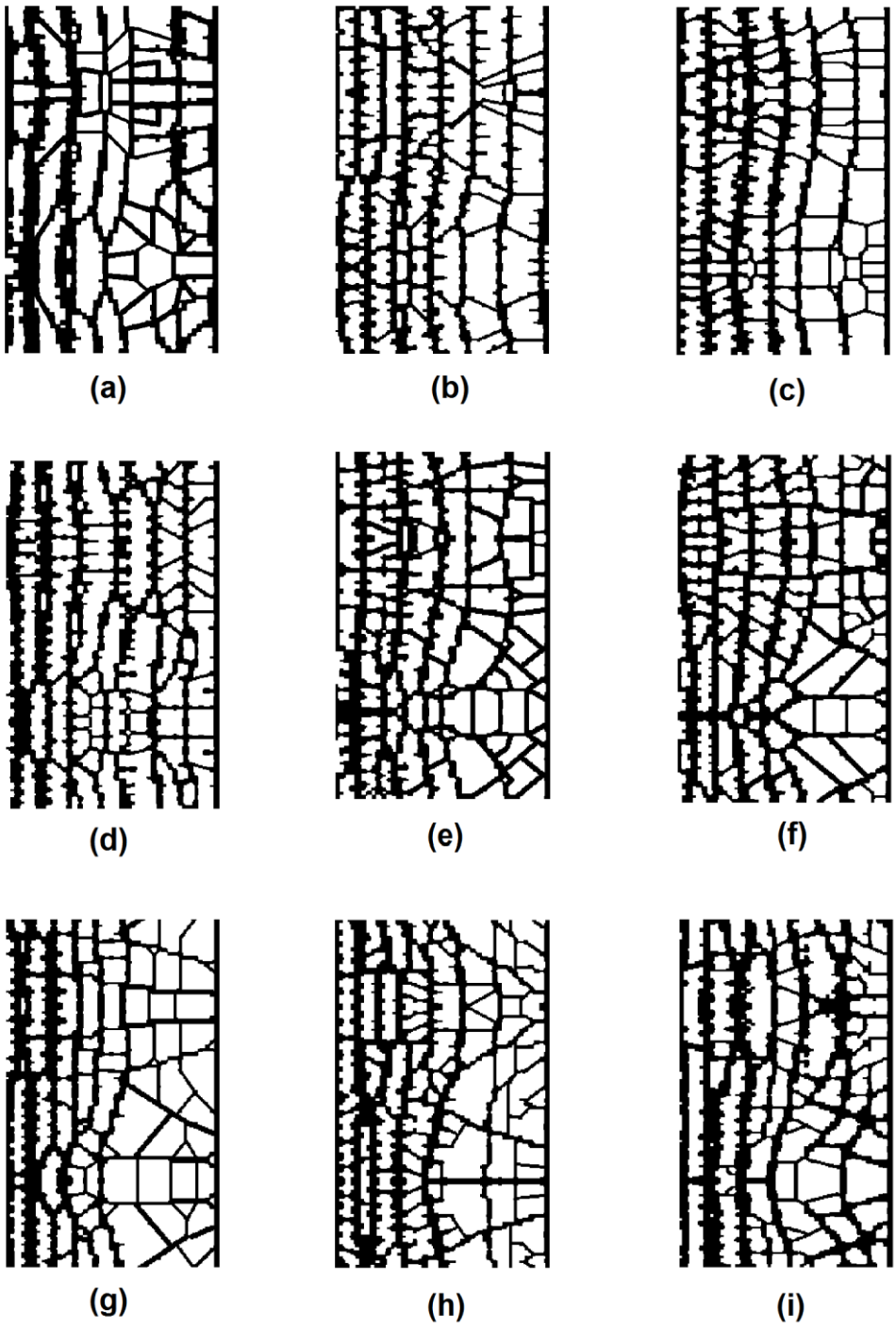

Figure 9

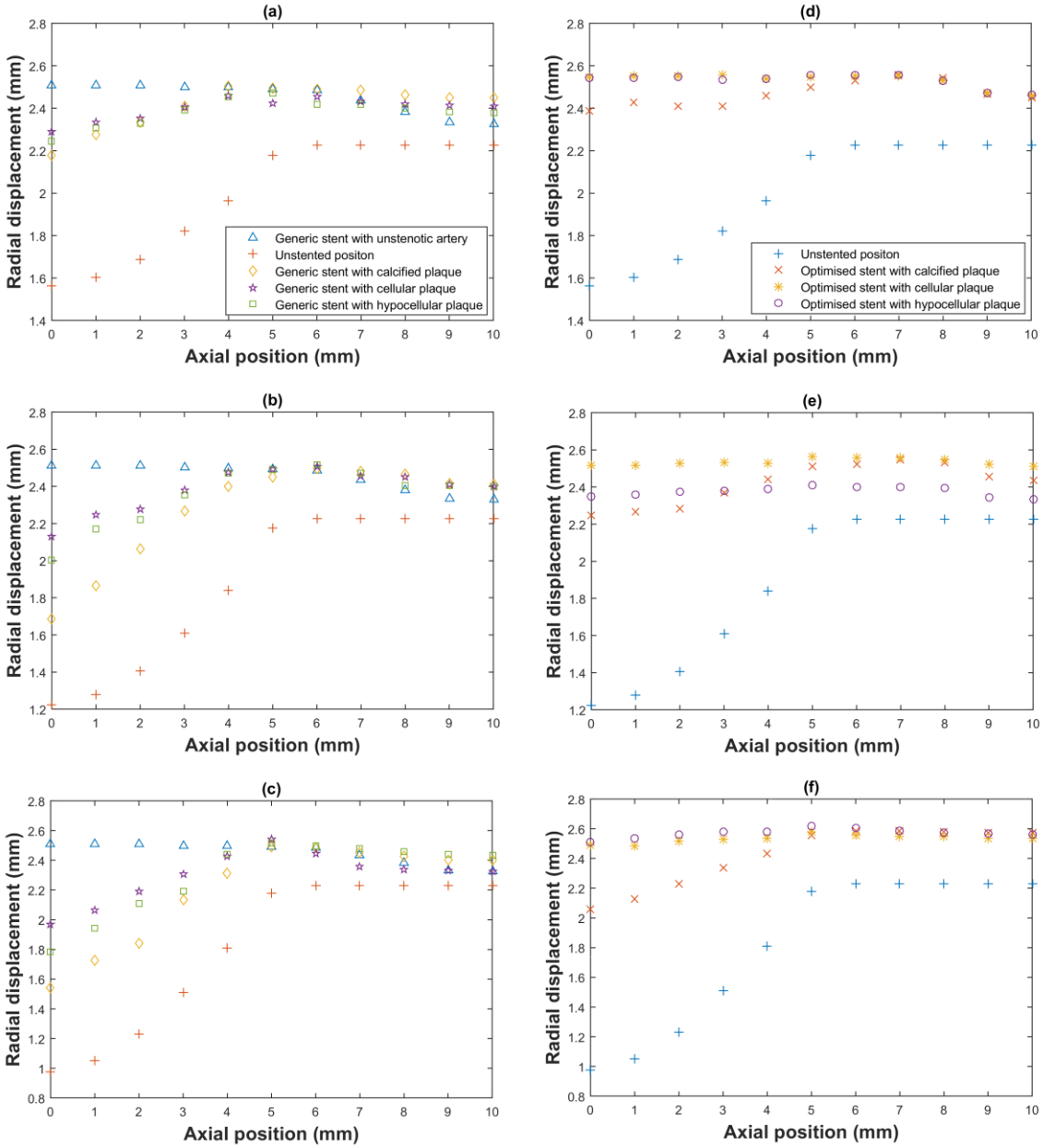

Figure 10

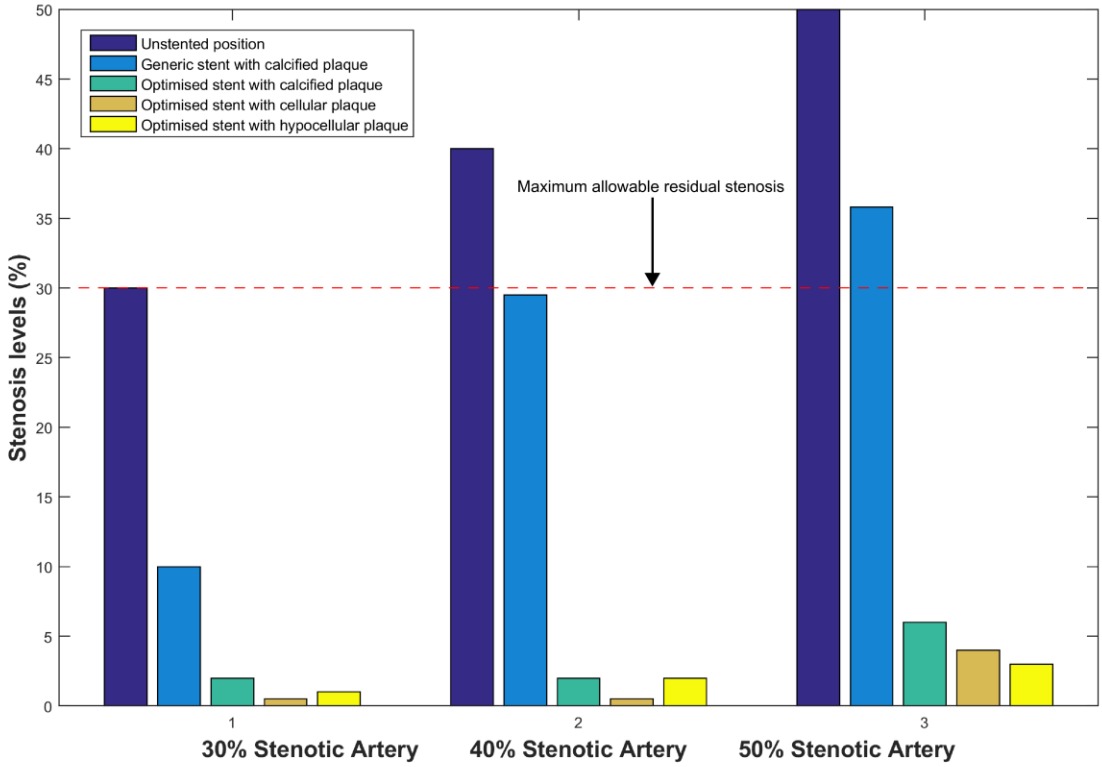

Figure 11

Table 1

Constants	Arterial Tissue (MPa)	Calcified Plaque (MPa)	Cellular Plaque (MPa)	Hypocellular Plaque (MPa)
C_{10}	0.025466	-0.4959	-0.8027	0.1651
C_{01}	-0.011577	0.5066	0.83163	0.01696
C_{20}	-0.000506	3.6378		
C_{11}	0.001703	1.19353	1.1578	0.9553
C_{30}	0.00165	4.7372		